Theory of electromagnetic response and collective excitations in antidots

S. A. Mikhailov* and V. A. Volkov
Institute of Radioengineering and Electronics, Russian Academy of Sciences, Mokhovaya Street, 11 Moscow, 103907 Russia
(Received 6 December 1994; revised manuscript received 8 September 1995)

The theory of collective excitations in a single antidot and in a system of interacting antidots is presented. The problem is solved within the framework of classical electrodynamics neglecting the nonlocal and retardation effects. It is shown that the spectrum of collective excitations in a single antidot consists of two branches. The first mode coincides with the single-particle cyclotron resonance $\omega=\omega_c$; the second one is the edge magnetoplasmon (EMP) mode. The EMP mode has the vanishing damping (in the collisionless approximation) only at $\omega<\omega_c$. At $\omega>\omega_c$ it decays on account of emission of two-dimensional (2D) bulk magnetoplasmons to the surrounding 2D medium. The induced electric potential and charge density of the EMP mode have the form of outgoing cylindrical waves at $\omega>\omega_c$. As a consequence, the interantidot interaction cannot be neglected in an array of antidots at $\omega>\omega_c$. Collective excitations in an array of interacting antidots are considered in the modified-dipole and effective-medium approximations. The results obtained explain the main features of the antidot excitation spectrum observed in recent experiments.

I. INTRODUCTION

The problem of far-infrared (FIR) response and collective excitations in low-dimensional electron systems in semiconductor microstructures has been of great interest in recent years. The remarkable progress of modern technology results in the creation of a number of man-made electronic systems of low dimensionality in semiconductors, such as quantum wells [two dimensional (2D)], quantum wires (1D), quantum dots (0D), rings, antidots, etc. The properties of single-particle and collective excitations in these artificial solid-state microstructures have been the subject of intensive experimental and theoretical investigations.

The problem of collective excitations in quantum dots (and classical disks) has been under consideration since 1983;[1-7] for a review see, e.g., Ref. 8. The FIR spectrum of dots in magnetic field B demonstrates two excitation branches, $\omega_+(B)$ and $\omega_-(B)$. The upper mode ω_+ starts from dimensional plasma resonance at $B=0$, and tends to the cyclotron frequency $\omega=\omega_c$ as B increases. The lower mode ω_- starts from the same frequency and decreases in frequency with increasing B. Circular polarization of the $+$ mode ($-$ mode) coincides with (is opposite to) the polarization of the cyclotron resonance (CR). As opposed to the homogeneous 2D electron layer, the CR line $\omega=\omega_c$ is not observed in dots due to the depolarization effect.[1]

The system of antidots is a reversed structure with respect to dots—this is a set of holes punched in a homogeneous 2D electron layer. In spite of the geometrical analogy the spectra of collective excitations in the systems of dots and antidots turn out to be distinctly different. Two strong absorption lines have been observed in FIR transmission spectrum of antidots;[9,10] see also Refs. 11 and 12. The upper antidot branch has a negative-B dispersion at small B, reaches its minimum, and then tends to the CR line as B increases. The lower antidot mode increases linearly with B at small B, achieves its maximum, and then decreases in frequency in strong B. These two modes demonstrate an exchange of oscillator strengths, indicating a physical coupling between them. Besides the two main branches, a weak CR line is observed in the spectrum of antidots as opposed to dots.

Theoretically, the spectrum of collective excitations in antidots was considered in Refs. 13–16. Fessatidis, Cui, and Kühn[13] considered the single antidot problem in the hydrodynamic approximation. They used the formal method of solving the problem, which did not allow them to clarify physical peculiarities of the antidot problem and to describe some of the experimentally observed features of the antidot spectrum (see the discussion in Sec. III). Wu and Zhao[14] considered the problem of a square antidot grid using the variational Wigner-Seitz approach, and obtained a good agreement with experimental data. Their theory,[14] however, is not applicable to the case of a single antidot. Lorke[15] simulated the dynamic conductivity of an antidot system in the classical model of ballistic electron motion, neglecting the collective effects completely. Tevosyan and Shikin[16] considered the problem of a single antidot in an artificial model with equilibrium electron density $n_s(r)\propto(r^2/R^2-1)^{1/2}$ growing linearly with r at $r\to\infty$.

In the present paper, we propose a theory of collective excitations in both a single antidot and a system of interacting antidots. We solve the problem within the framework of classical electrodynamics, neglecting the spatial dispersion and retardation effects. For a single antidot we use the model with the steplike equilibrium electron density $n_s(r)=n_s\Theta(r-R)$, and discuss the influence of the finite transition layer at the boundary of the antidot on the spectrum of collective modes. We find asymptotes of the induced potential, response function, and polarizability of a single antidot (Sec. III). We argue that, contrary to the system of dots, an interantidot interaction

cannot be neglected in the system of antidots. In an array of antidots (Sec. IV), we calculate the response function of a system in the modified-dipole (MDA) and effective-medium (EMA) approximations. A special section (Sec. II) is devoted to a qualitative discussion of the main physical features of the problem. The main results are formulated in Sec. V.

II. QUALITATIVE CONSIDERATION

The qualitative difference between the collective excitation spectra of a single dot and single antidot can be understood from a simple physical consideration. In a dot, electrons are confined in a finite area of 2D space by an external potential. An electric field of external electromagnetic waves induces an oscillating dipole moment in a dot, the value of which depends on FIR frequency ω and magnetic field B. When the frequency of the external wave coincides with the frequency of the dimensional magnetoplasma resonance, the dipole moment $\mathbf{P}$ diverges and a collective plasma mode is excited.

In the case of a single antidot the situation is more complicated. Electrons are not now confined in a finite area of 2D space. An oscillating dipole moment $\mathbf{P}$ induced near an antidot by an external electromagnetic wave is immersed into a 2D polarizable medium—a 2D electron gas. The FIR response of a single antidot is therefore affected by the screening properties of 2D electrons in a magnetic field. The dielectric permittivity of a 2D electron gas $\varepsilon(q,\omega)$ essentially depends on the relation between ω and the cyclotron frequency $\omega_c=eB/mc$. If $\omega<\omega_c$, the dielectric function $\varepsilon(q,\omega)$ is positive, and screening decreases the induced dipole moment only. A more dramatic effect is the case at $\omega>\omega_c$. The dielectric function $\varepsilon(q,\omega)$ changes its sign at $\omega>\omega_c$, and vanishes at the frequency of 2D bulk magnetoplasmons

$$\omega_{\rm mp}(q)=[\omega_c^2+\omega_p^2(q)]^{1/2}\ ,$$
$$\omega_p(q)=(2\pi n_s e^2 q/m\kappa)^{1/2}\ ; \tag{1}$$

here $\omega_p(q)$ is the frequency of a 2D plasmon with wave vector q at $B=0$. When the frequency ω of the oscillating dipole moment coincides with $\omega_{\rm mp}(q)$, the 2D bulk magnetoplasmon with the wave vector q is emitted into the surrounding 2D medium. The collective modes of a single antidot therefore have a strong nondissipative (emissive) damping at $\omega>\omega_c$. Emissive damping of this type is obviously not the case in a single dot.

The emission of 2D bulk magnetoplasmons by a single antidot in a 2D plane is quite similar to the radiation of transverse electromagnetic waves by an oscillating dipole in a 3D plasma. The spectrum of electromagnetic waves in plasma $\omega=[\omega_p^2+(cq)^2]^{1/2}$ has a gap equaled to the bulk plasma frequency ω_p. Therefore, the oscillating dipole radiates electromagnetic waves at $\omega>\omega_p$, and does not radiate at $\omega<\omega_p$. Similarly, due to the gap ω_c in the spectrum of bulk 2D magnetoplasmons (1), the oscilating antifot dipole emits 2D bulk magnetoplasmons $\omega>\omega_c$, and does not emit at $\omega<\omega_c$.

The effect considered leads to an important conclusion relative to the role of interantidot interaction in an array of antidots. In an array of dots, an interdot interaction can be taken into account in the dipole approximation, and normally is negligible if the separation between dots exceeds several dot radii.[17] In an array of antidots, interantidot interaction can be neglected only at $\omega\ll\omega_c$, when the charge density fluctuation is localized near the antidots. When the frequency ω tends to the cyclotron frequency and exceeds it, the overlapping of neighbor antidot potentials is considerably increased due to 2D bulk magnetoplasmon emission. Therefore *the interaction between antidots must be taken into account even in a scarce lattice of antidots.*

The wave vector of induced 2D bulk magnetoplasmon is determined by equality $\omega=\omega_{\rm mp}(q)$, where ω is the frequency of external electromagnetic wave. At $\omega>\omega_c$, the absorption spectrum of a single antidot is thus continuous. In an ordered lattice of antidots, coherence effects give rise to preferential excitation of 2D bulk magnetoplasmons with wave vectors $\mathbf{q}=\mathbf{G}_n$, where $\mathbf{G}_n$ are the reciprocal-lattice vectors. Thus we come to the known picture of 2D bulk magnetoplasmon excitation via the spatial grating (or grid) imposed on the homogeneous 2D electron layer.

III. SINGLE ANTIDOT IN EXTERNAL ac ELECTRIC FIELD

A. Basic equations

Let the 2D electron layer with a single antidot be placed at the plane $z=0$, the magnetic field B be directed along the z axis, the background dielectric permittivity be κ_1 above the 2D layer (at $z>0$) and κ_2 below it (at $z<0$), and the external electric field be described by the potential $\varphi_{\rm ext}(\mathbf{r},t)=\varphi_{\pm}^{\rm ext}(r)\exp(\pm i\theta-i\omega t)$, where $r=(x,y)$ is the 2D vector, and $\varphi_{\pm}^{\rm ext}(r)=-E_{\pm}^0 r/\sqrt{2}$ and $E_{\pm}^0=(E_x^0\mp iE_y^0)/\sqrt{2}$ are the field amplitudes with polarization coinciding with $(+)$ and opposite to $(-)$ the polarization of the CR. Neglecting the retardation[18] and spatial dispersion effects, charge-density fluctuations are described by Poisson and continuity equations and Ohm's law with local conductivity tensors $\sigma_{\alpha\beta}(r,\omega)=\sigma_{\alpha\beta}(\omega)\Theta(r-R)$, $\{\alpha,\beta\}=\{x,y\}$, $\sigma_{xx}=\sigma_{yy}$, and $\sigma_{xy}=-\sigma_{yx}$. To explicitly allow for the screening of the self-consistent electric field, we present the conductivity tensor in the form $\sigma_{\alpha\beta}(r,\omega)=\sigma_{\alpha\beta}(\omega)-\sigma_{\alpha\beta}(\omega)\Theta(R-r)$, and obtain the following equation for induced $\varphi_{\rm ind}$ and total $\varphi_{\rm tot}$ electric potentials:

$$\nabla_3[\kappa(z)\nabla_3\varphi_{\rm ind}(\mathbf{r},z)]+[4\pi i\sigma_{xx}(\omega)/\omega]\delta(z)\Delta_2\varphi_{\rm ind}(r,0)=-4\pi\delta\rho(\mathbf{r})\delta(z)\ . \tag{2}$$

Here ∇_3 is the 3D nabla, Δ_2 is the 2D Laplacian, and

$$\delta\rho(\mathbf{r})=-(i/\omega)\partial_\alpha[\sigma_{\alpha\beta}(\omega)\Theta(R-r)\partial_\beta\varphi_{\rm tot}(\mathbf{r},0)] \tag{3}$$

is nonzero inside the antidot hole ($r<R$), $\partial_\alpha\equiv\partial/\partial x_\alpha$. We thus replace the problem of a single antidot with the problem of a single dot with *negative* electron density

placed in a homogeneous 2D electron layer with a background conductivity $\sigma_{\alpha\beta}(\omega)$.

With the help of the Fourier-Bessel transform, Eq. (2) is rewritten in the integral form

$$\varphi_{\pm}^{\rm ind}(r)=(\pi/\kappa l)\int_0^{\infty} r'dr' L(r,r';l)\delta\rho_{\pm}(r') , \tag{4}$$

where integration is performed over the region $0<r\le R$ [see Eq. (3)], and the kernel

$$L(r,r';l)=2l\int_0^{\infty}\frac{dq}{\varepsilon(q,\omega)}J_1(qr)J_1(qr') \tag{5}$$

depends explicitly on dielectric function of the 2D layer

$$\varepsilon(q,\omega)=1+ql(\omega)=1+\frac{2\pi i\sigma_{xx}(\omega)q}{\omega\kappa}$$
$$=1+\frac{i\omega_p^2(q)\tau(1-i\omega\tau)}{\omega[(1-i\omega\tau)^2+(\omega_c\tau)^2]} . \tag{6}$$

Here $\kappa=(\kappa_1+\kappa_2)/2$, the length $l=l(\omega)$ is proportional to the polarizability $\chi_{xx}(\omega)=i\sigma_{xx}(\omega)/\omega$ of the 2D layer [in strong B, $|l(\omega)|$ determines the scale of localization of edge magnetoplasmon (EMP) charge near the edge of the 2D system[7,19]], τ is momentum relaxation time, and the Drude formula for $\sigma_{xx}(\omega)$ is used in the last equality. The properties of kernel $L(r,r';l)$ are listed in the Appendix.

Substituting $\delta\rho$ into Eq. (4), we reduce the problem to an integral equation for $\varphi_{\pm}^{\rm ind}(r)$,

$$\varphi_{\pm}^{\rm ind}(r)=\frac{i\pi\sigma_{\pm}(\omega)}{\omega\kappa l}\varphi_{\pm}^{\rm tot}(R)L(r,R;l)$$
$$-\tfrac{1}{2}\int_0^{\infty}dr' L(r,r';l)\hat{D}\{\varphi_{\pm}^{\rm ind}(r')\} , \tag{7}$$

which is completely equivalent to Eq. (2). Here $\sigma_{\pm}(\omega)\equiv\sigma_{xx}(\omega)\pm i\sigma_{xy}(\omega)$ and

$$\hat{D}\{\varphi(r)\}=\partial_r[r\Theta(R-r)\partial_r\varphi(r)]$$
$$-[\varphi(r)/r]\partial_r[r\Theta(R-r)] . \tag{8}$$

With the help of Eq. (7) one can find exact asymptotes of the induced potential and charge density at $r\gg R$, as well as the response function of a single antidot.

B. Asymptotes of induced potential and charge density at $r\gg R$

Since the operator $\hat{D}$ is zero at $r>R$, the asymptotic behavior of the induced potential at $r\gg R$ is determined by asymptotes (A1) and (A2) of the kernel $L(r,R;l)$, and depends on the ratio $R/l(\omega)$. At $\omega<\omega_c$ the dielectric function $\varepsilon(q,\omega)$ is positive at all $q>0$, and at $r\gg R$ we have:

$$\varphi_{\pm}^{\rm ind}(r)=\frac{2i\sigma_{\pm}(\omega)R}{\omega\kappa l^2}\varphi_{\pm}^{\rm tot}(R)F(r/l)$$
$$\approx\frac{i\pi\sigma_{\pm}(\omega)R}{\omega\kappa r(r+l)}\varphi_{\pm}^{\rm tot}(R), \quad r\gg R , \tag{9}$$

$$\rho_{\pm}(r)\approx\frac{i\sigma_{\pm}(\omega)Rl}{2\omega}\frac{3r+l}{r^2(r+l)^3}\varphi_{\pm}^{\rm tot}(R), \quad r\gg R \tag{10}$$

[we use the interpolation formula (A4) here]. When the frequency is small, $\omega\ll\omega_c$, and the magnetic field is strong, $\omega_c\gg\omega_p(q=1/R)$, the length $l(\omega)$ is positive (we consider the collisionless limit for simplicity) and much smaller than the antidot radius R, $|l(\omega)|\ll R$. Under these conditions, the charge density of the excitation (EMP) is strongly localized near the boundary of the antidot, $\rho_{\pm}(r)\propto 1/r^4$, and the induced potential has the dipole character $\varphi_{\pm}^{\rm ind}(r)\propto 1/r^2$. With increasing frequency the length $l(\omega)$ increases and at $0<(\omega_c^2-\omega^2)<\omega_p^2(1/R)$ becomes larger than R. At $l(\omega)/R\to+\infty$ the single antidot mode displays the tendency to delocalization: $\varphi_{\pm}^{\rm ind}(r)\propto 1/r$, and $\rho_{\pm}(r)\propto 1/r^2$, at $R\ll r\ll|l(\omega)|$.

When ω exceeds the cyclotron frequency ω_c, the length $l(\omega)$ changes its sign and $\varepsilon(q,\omega)$ vanishes at the wave vector $q=-1/l(\omega)$, corresponding to the emission of 2D bulk magnetoplasmons with the frequency ω. The induced potential and charge density acquire the form of the outgoing cylindrical wave at $\omega>\omega_c$ [see Eqs. (7) and (A1)],

$$\varphi_{\pm}^{\rm ind}(r)\propto H_1^{(1)}(-r/l), \quad \rho_{\pm}(r)\propto H_1^{(1)}(-r/l) ,$$
$$r\gg R, \quad R/l(\omega)<0 ; \tag{11}$$

here $H_1^{(1)}$ is the Hankel function.

Thus the charge-density fluctuation is localized near an antidot only at $\omega<\omega_c$. An induced dipole moment of excitation is finite and equal to

$$P_{\pm}\equiv(P_x\mp iP_y)/\sqrt{2}$$
$$=\sqrt{2}\pi\int_0^{\infty}r^2\rho_{\pm}(r)dr$$
$$=\frac{\sqrt{2}\pi i\sigma_{\pm}(\omega)R}{\omega}\cdot\varphi_{\pm}^{\rm tot}(R), \quad \omega<\omega_c . \tag{12}$$

At $\omega>\omega_c$ the charge-density wave (11) is emitted from the antidot, and the dipole moment (12) diverges.

C. Response function and polarizability of a single antidot

We define the response function $\zeta_{\pm}(\omega)$ of a single antidot as follows:

$$\zeta_{\pm}(\omega)=[\varphi_{\pm}^{\rm ext}/\varphi_{\pm}^{\rm tot}]_{r=R,z=0} . \tag{13}$$

Zeros of functions $\zeta_{\pm}(\omega)$ determine the spectrum of collective excitations in the antidot.

To find $\zeta_{\pm}(\omega)$ we solve the integral equation (7) by the method of successive approximations. In the first approximation, we neglect the integral term in (7) and obtain

$$\zeta_{\pm}(\omega,\omega_c)\equiv\zeta_{\mp}(\omega,-\omega_c)$$
$$=1-\frac{i\pi\sigma_{\pm}(\omega)}{\omega\kappa}\left\{l(\omega)+\frac{8R}{3\pi[1+\gamma(R/l)]}\right\}^{-1} ; \tag{14}$$

the function $\gamma(z)$, Eq. (A6), is small at $|z|\ll 1$, and slowly (logarithmically) increases with z.

The accuracy of the first-order approximation has been estimated numerically. We have found that the correction to $\zeta_{\pm}(\omega)$, Eq. (14), tends to zero at $R/l \to 0$ and does not exceed 7% at $-1.4 < R/l < 25$; at $R/l > 25$ the same accuracy can be obtained if we replace $\gamma(R/l)$ in Eq. (14) by $\gamma(2R/l)$. The condition $-1.4 < R/l < \infty$ corresponds to the frequency range $\omega^2 < \omega_c^2 + 1.4\omega_p^2(1/R)$, in which the collective excitation branches of interest lie.

From Eqs. (12) and (13) one can find the polarizability $\alpha_{\pm}(\omega) \equiv P_{\pm}/E_{\pm}^0$ of a single antidot:

$$\alpha_{\pm}(\omega,\omega_c) \equiv \alpha_{\mp}(\omega,-\omega_c) = -\frac{i\pi\sigma_{\pm}(\omega)/R^2}{\omega\zeta_{\pm}(\omega)}, \quad \omega < \omega_c \ . \tag{15}$$

D. Excitation spectrum of a single antidot

Due to the effect of emission of 2D bulk magnetoplasmons by the antidot dipole, the functions $\zeta_{\pm}(\omega)$ have no real zeros at $\omega > \omega_c$ [the function $\gamma(z)$ is complex at $z < 0$], and antidot modes have strong emissive damping. At $0 < \omega \le \omega_c$ the functions $\zeta_-(\omega)$ and $\zeta_+(\omega)$ have no and two zeros, respectively. Thus there are two + polarized collective modes in a single antidot. The first collective mode $\omega_{CR}(B) = \omega_c$ coincides with the single-particle CR. The frequency of the second (EMP) branch is determined by the equation

$$\omega_{EMP}(B) = -(\omega_c/2) + \sqrt{(\omega_c/2)^2 + \omega_0^2[1+\gamma(R/l)]} \ , \tag{16}$$

where

$$\omega_0^2 = 3\pi^2 n_s e^2/8m\kappa R \ . \tag{17}$$

Magnetic-field dependencies $\omega_{CR}(B)$ and $\omega_{EMP}(B)$ are shown in Fig. 1. At $\omega_c/\omega_0 \approx 0.8$, the EMP mode (the solid curve) has a weak maximum and enters the continuum of 2D bulk magnetoplasmon states (hatched region in Fig. 1) at $\omega_c = \omega_0/\sqrt{2}$. In strong B, the EMP mode

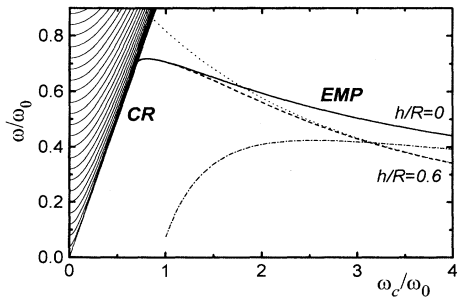

FIG. 1. Two modes of the single antidot excitation spectrum $\omega_{CR}(B)$ and $\omega_{EMP}(B)$. The EMP mode is shown by the solid curve in the case of a sharp edge of a 2D layer ($h/R = 0$), and by the dashed curve in the case of a smooth edge with $h/R = 0.6$. The logarithmic asymptote (18) is shown by the dashed-dotted curve. The dotted curve corresponds to Eq. (16), with l replaced by h. The hatched region at $\omega > \omega_c$ is the continuum of the 2D bulk magnetoplasmons.

$\omega_{EMP}(B)$ decreases in frequency with B and tends to the asymptote

$$\omega_{EMP}(B) = (2\sigma_{yx}^0/\kappa R)[\ln(2R/l_0) - \psi(\tfrac{3}{2})], \quad \omega_c \gg \omega_0 \tag{18}$$

(the dash-dotted curve). Here $\sigma_{yx}^0 = n_s e^2/m\omega_c$, $l_0 = \mathrm{Re}\, l(\omega)|_{\omega/\omega_c \to 0} = 2\pi n_s e^2/m\kappa\omega_c^2$ [if $R/l_0 > 25$, l_0 should be replaced by $l_0/2$], and $\Psi(z)$ is the digamma function $\Psi(\frac{3}{2}) = 0.037$.

The logarithmic factor $\ln(R/l)$ in Eq. (18) is a typical property of EMP's running along the sharp edge of the 2D layer.[7,19] In 2D systems with a smooth transition layer (width h) near the edge, the length l in (16) should be replaced by $\sqrt{l^2+h^2}$. The dashed curve in Fig. 1 demonstrates the influence of the transition layer width on the EMP spectrum at $h/R = 0.6$.[20] The asymptote $\omega_{EMP}(B) \propto (1/B)\ln(B)$ in the strong field is replaced by $\omega_{EMP}(B) \propto 1/B$ in this case. The dotted curve shows spectrum (16) with l replaced by h.

It should be noted here that the single antidot problem was considered within the same model in Ref. 13. Contrary to our approach, Fessatidis, Cui, and Kühn[13] wrote the Poisson equation in the usual form, with $\rho(\mathbf{r})$ on the right-hand side of the equation. As a result, their kernel $L(r,r')$ does not depend on $\varepsilon(q,\omega)$, and the integral in Eq. (4) is taken in the limits $R \le r < \infty$. Then they solved the problem numerically, obtained a real branch of excitation spectrum at $\omega > \omega_c$ and did not find the effect of the 2D bulk magnetoplasmon emission. From a mathematical point of view, the formal numerical integration of a charge density in the limits from R to infinity can be in error since, as seen from exact asymptotes [Eq. (11)], $\rho_{\pm}(r)$ has a slowly descending oscillating tail at $r \gg R$. The validity of the theory[13] is thus restricted by the region $\omega < \omega_c$.

IV. COLLECTIVE EXCITATIONS IN AN ARRAY OF ANTIDOTS

One can expect that the excitation spectrum of a single antidot is essentially modified in an array of antidots due to the interantidot interaction. Two collective modes of a single antidot spectrum, $\omega_{CR}(B)$ and $\omega_{EMP}(B)$, have the same (+) polarization and intersect at $\omega = \omega_c = \omega_0/\sqrt{2}$. Interantidot interaction will result in the mode repulsion at the intersection point.[21] This modifies the spectrum of modes at $\omega < \omega_c$. At $\omega > \omega_c$, the coherence effects increase the emissive damping of antidot modes when the wave vector of the excited 2D magnetoplasmon coincides with one of the reciprocal-lattice vectors, and suppresses it in the opposite case. This will modify the spectrum of a single antidot at $\omega > \omega_c$.

The influence of interantidot interaction is different in different frequency ranges. At $\omega < \omega_c$ it is weak and can be included in the dipole approximation [which we modify with an account of the actual asymptote (9) of $\varphi_{\pm}^{ind}(r)$]. At $\omega > \omega_c$, an interaction is not weak, and one needs more elaborate approaches. Below we use EMA (see also Ref. 22), which allows us to describe qualitatively the behavior of both excitation branches in a system of interacting antidots.

A. Modified-dipole approximation

In both approximations, we calculate the effective conductivity of a system which determines the relation between the macroscopically averaged electric current and the field,

$$\langle j_{\pm}(\omega,\mathbf{r})\rangle_{\text{sample}}=\sigma_{\pm}^{\text{eff}}(\omega)\langle E_{\pm}(\omega,\mathbf{r})\rangle_{\text{sample}} . \tag{19}$$

In an infinite system $\langle E_{\pm}(\omega,\mathbf{r})\rangle_{\text{sample}}=E_{\pm}^{0}$. The averaged current is expressed via the geometrical filling factor of antidots f and the total electric field averaged over an area of one antidot $\langle E_{\pm}^{\text{tot}}(\omega,\mathbf{r})\rangle_{\text{antidot}}$. From Eq. (13) it follows that

$$\langle E_{\pm}^{\text{tot}}(\omega,\mathbf{r})\rangle_{\text{antidot}}=E_{\pm}^{\text{loc}}/\zeta_{\pm}(\omega) , \tag{20}$$

where $E_{\pm}^{\text{loc}}$ is the local electric field acting on antidots. Modifying the standard dipole approximation with an account of the actual asymptote $\varphi_{\pm}^{\text{ind}}(r)\propto F(r/l)$ at $r\gg R$ [Eq. (9)], we obtain the effective conductivity of a square lattice of antidots with period a:

$$\sigma_{\pm}^{\text{eff}}(\omega)=\sigma_{\pm}(\omega)-\frac{f\sigma_{\pm}(\omega)}{\zeta_{\pm}(\omega)\{1-[2\pi\alpha_{\pm}(\omega)/\eta\kappa a l^{2}]F(\pi a/\eta l)\}} . \tag{21}$$

Here $f=\pi R^{2}/a^{2}$ and

$$\eta=\tfrac{1}{2}\sum_{(i,j)\neq(0,0)}(i^{2}+j^{2})^{-3/2}=4.516 .$$

The MDA expression (21) is valid at $\omega\leq\omega_c$ and $R/a\ll 1$; in the limit $a\gg|l(\omega)|$ it coincides with that obtained in the standard dipole approximation.

The excitation spectrum of a system is determined by poles of $\sigma_{\pm}^{\text{eff}}(\omega)$ and, as seen from Eq. (21), is presented by a single-particle and collective contributions. The single-particle excitations are determined by poles of $\sigma_{\pm}(\omega)$; this gives the CR mode $\omega=\pm\omega_c$. The collective excitations are determined by zeros of the denominator in Eq. (21). In the limit $a\to\infty$ they coincide with zeros of response functions $\zeta_{\pm}(\omega)$; see Sec. III. Interantidot interaction modifies the single antidot spectrum, as shown in Fig. 2(a) at different values of f. In strong B the charge density of the +-polarized collective EMP-like mode $\omega_{\text{low}}^{(+)}(B)$ is strongly localized near antidot boundaries, and the frequency $\omega_{\text{low}}^{(+)}(B)$ tends to $\omega_{\text{EMP}}(B)$; in small B $\omega_{\text{low}}^{(+)}(B)$ is a linear function of magnetic field with a slope depending on f:

$$\omega_{\text{low}}^{(+)}(B)=\begin{cases}\omega_c(1-f)/(1+f) , & \omega_c\ll\omega_0\\ (2\sigma_{yx}^{0}/\kappa R)[\ln(2R/l_0)-\psi(\frac{3}{2})-(\eta/2)(f^{3}/\pi)^{1/2}] , & \omega_c\gg\omega_0 .\end{cases} \tag{22}$$

The single-particle model $\omega=\omega_c$ labeled by CR is also shown in Fig. 2(a). Figure 2(b) demonstrates the influence of the transition layer near the edge of the antidot hole on the spectrum of the low-frequency mode in the MDA at $f=0.087$ and $h/R=0.6$.[20] For comparison, the single antidot spectra at $h/R=0$ and $h/R=0.6$ are also shown.

In Fig. 3(a) the low-frequency MDA curve $\omega_{\text{low}}^{(+)}(B)$ is shown with experimental points obtained in Ref. 9 with sample (b) ($n_s=2.5\times10^{12}$ cm^{-2}, $a=300$ nm, $R=50$ nm, and $h\approx30$ nm). The value of the effective mass $m=0.06m_0$ has been found from CR data. Then the curve $\omega_{\text{low}}^{(+)}(B)$ has been fitted by variation of ω_0. The thus-obtained value of ω_0 equals $\omega_0^{\text{MDA}}=1.8\times10^{13}$ s^{-1}. The calculated value of ω_0, Eq. (17), depends on the radius of the antidot hole. Using for R two values, $R=50$ nm (the radius of etched hole) and $R+h=80$ nm (the etched hole radius plus the lateral edge depletion with h), we obtain $\omega_0^{\text{calc}}(R=50\text{ nm})=2.38\times10^{13}$ s^{-1} and $\omega_0^{\text{calc}}(R=80\text{ nm})=1.88\times10^{13}$ s^{-1}. Thus the MDA gives a good quantitative agreement with experimental data[9] for the low-frequency excitation branch in an array of antidots.

B. Effective-medium approximation

An account of interantidot interaction at $\omega>\omega_c$ is a more complicated problem, since the interaction is not

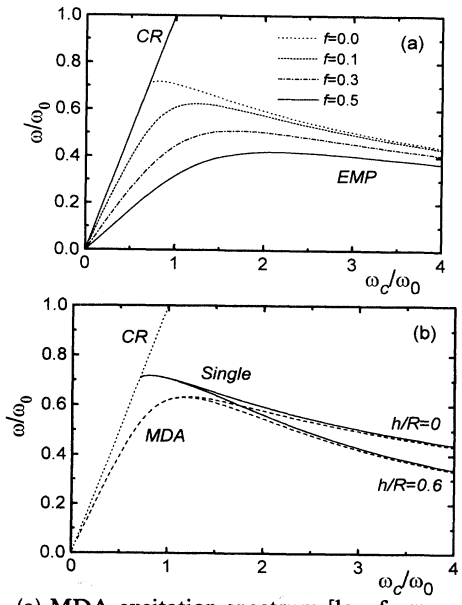

FIG. 2. (a) MDA excitation spectrum [low-frequency EMP-like mode $\omega_{\text{low}}^{(+)}(B)$] in the square lattice of antidots at different f and at $h/R=0$ (sharp edge). (b) MDA low-frequency branch at the sharp edge ($h/R=0$) and smooth edge ($h/R=0.6$) of the antidot hole at $f=0.087$. The single antidot spectra at $h/R=0$ and 0.6 are also shown. CR labels the single-particle cyclotron resonance mode.

weak. To obtain a qualitative description of the high-frequency antidot mode we use the EMA. In the EMA, we replace the problem of an array of interacting antidots immersed in the medium with conductivity $\sigma_{\pm}(\omega)$ by the problem of a single antidot immersed in the effective medium with conductivity $\sigma_{\pm}^{\rm eff}(\omega)$. This allows us to write, instead of Eq. (20);

$$\langle E_{\pm}^{\rm tot}(\omega,\mathbf{r})\rangle_{\rm antidot}=E_{\pm}^{0}/\zeta_{\pm}^{\rm eff}(\omega)\ . \tag{23}$$

The self-consistent EMA equation for $\sigma_{\pm}^{\rm eff}(\omega)$ then assumes the form

$$\sigma_{\pm}^{\rm eff}(\omega)=\sigma_{\pm}(\omega)-\frac{f\sigma_{\pm}(\omega)}{1-\{i\pi\sigma_{\pm}^{\rm eff}(\omega)/\omega\kappa[l_{\rm eff}(\omega)+8R/3\pi(1+\gamma(R/l_{\rm eff}))]\}}, \tag{24}$$

where $l_{\rm eff}(\omega)=2\pi i\sigma_{xx}^{\rm eff}(\omega)/\omega\kappa$. The solution of Eq. (24) can be essentially simplified if we replace the weak (logarithmic) function $\gamma(R/l_{\rm eff})$ by a value γ^* independent of frequency and magnetic field. This simplification can be justified in a twofold manner. First, as has been seen above, the function γ does not actually depend on the length l when the finite width of transition layer h near the edge of antidot is taken into account. Second, we are interested in the spectrum of collective excitations of a system. This is determined by the poles of effective conductivity $\sigma_{\pm}^{\rm eff}(\omega)$ and hence, by the poles of $l_{\rm eff}(\omega)$. Near the poles of $l_{\rm eff}(\omega)$ the function $\gamma(R/l_{\rm eff})$ tends to zero [Eq. (A6)], and can be neglected.

With $\gamma(R/l_{\rm eff})\approx\gamma^*=$const the EMA equation (24) is solved analytically. The solution written in terms of functions $\varepsilon_{\pm}(\omega)\equiv 1+[3\pi^2 i\sigma_{\pm}(\omega)(1+\gamma^*)]/4\omega\kappa R$ has the form

$$\varepsilon_{\pm}^{\rm eff}(\omega)\equiv 1+\frac{3\pi^2 i\sigma_{\pm}^{\rm eff}(\omega)(1+\gamma^*)}{4\omega\kappa R}$$
$$=\frac{\{(\varepsilon_{\pm}-1)(\varepsilon_{\mp}+1)-2f(\varepsilon_{+}\varepsilon_{-}-1)\}+\sqrt{(\varepsilon_{+}+1)^2(\varepsilon_{-}+1)^2-4f(1-f)(\varepsilon_{+}^2-1)(\varepsilon_{-}^2-1)}}{2\{(\varepsilon_{\mp}+1)+f(\varepsilon_{\pm}-\varepsilon_{\mp})\}}\ . \tag{25}$$

The dispersion law for antidot modes is determined by poles of $\sigma_{\pm}^{\rm eff}(\omega)$:

$$1-\frac{1-f}{\Omega(\Omega\pm\Omega_c)}-\frac{f}{\Omega(\Omega\mp\Omega_c)}=0\ ; \tag{26}$$

here $\Omega=\omega/\omega_0^*$, $\Omega_c=\omega_c/\omega_0^*$, and $(\omega_0^*)^2=\omega_0^2(1+\gamma^*)$; the upper (lower) sign corresponds to the + (−) polarized modes.

Figure 4 demonstrates the FIR absorption and excitation spectra of a system of antidots in the EMA. Figure 4(a) shows the frequency dependence of $\mathrm{Re}\sigma_{xx}^{\rm eff}(\omega)\equiv\mathrm{Re}\,[\sigma_{+}^{\rm eff}(\omega)+\sigma_{-}^{\rm eff}(\omega)]/2$ at $f=0.1$, $\omega_0\tau=10$, and several dimensionless magnetic fields. The resonance frequencies found from Eq. (26) are shown in Fig. 4(b) as a function of B. There are two modes $\omega_{\rm up}^{(+)}(B)$ and $\omega_{\rm low}^{(+)}(B)$ with a relatively large oscillator strength and + polarization (coinciding with the CR one), and one mode $\omega_{\rm up}^{(-)}(B)$ with the opposite (−) polarization and a small oscillator strength. The behavior of modes $\omega_{\rm up}^{(\pm)}(B)$ and $\omega_{\rm low}^{(+)}(B)$ in small and strong magnetic fields is determined by expressions

$$\Omega_{\rm up}^{(\pm)}(\Omega_c)=\begin{cases}1\mp(\frac{1}{2}-f)\Omega_c, & \Omega_c\ll 1\\ \sqrt{\Omega_c^2+1\mp(1-2f)}, & \Omega_c\gg 1\ ,\end{cases} \tag{27}$$

$$\Omega_{\rm low}^{(+)}(\Omega_c)=\begin{cases}(1-2f)\Omega_c, & \Omega_c\ll 1\\ (1-2f)/\Omega_c, & \Omega_c\gg 1\ .\end{cases} \tag{28}$$

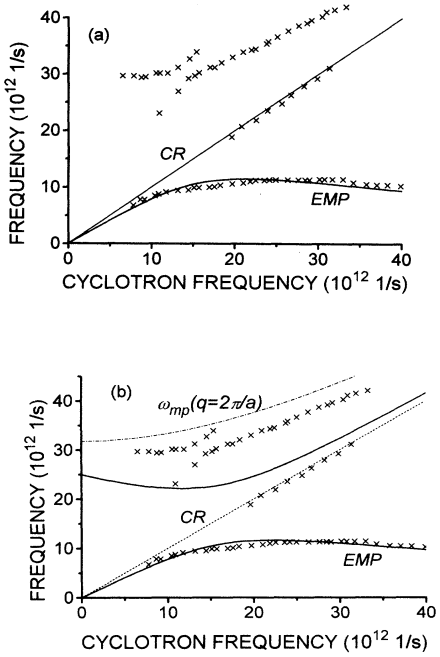

FIG. 3. Experimental points (crosses) from Ref. 9, sample (b), with theoretical curves: (a) MDA single-particle mode (CR) and collective mode $\omega_{\rm low}^{(+)}(B)$ (labeled EMP in strong B); (b) EMA collective modes $\omega_{\rm low}^{(+)}(B)$ and $\omega_{\rm up}^{(+)}(B)$ and 2D bulk magnetoplasmon excitation branch $\omega_{\rm mp}(q=2\pi/a)$ (dashed-dotted curve).

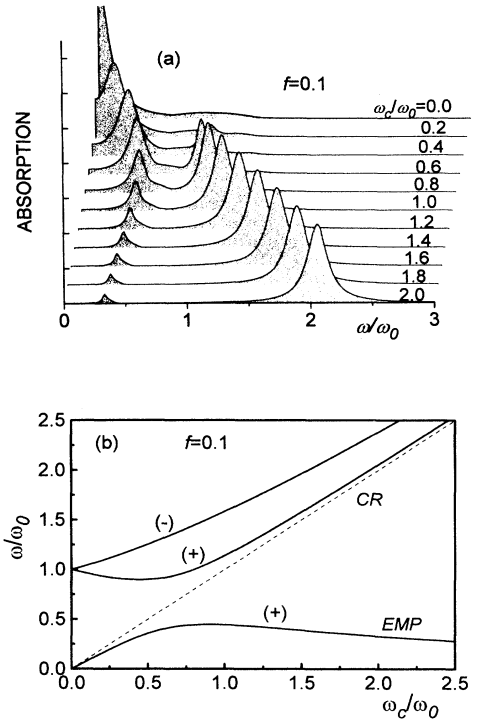

FIG. 4. FIR absorption (a) and excitation (b) spectra of a system of antidots in the EMA at $f=0.1$. (+) and (−) signs in (b) label the polarization of modes.

The low-frequency + polarized mode takes its maximum value $(\Omega_{\rm low}^{(+)})_{\rm max}=\sqrt{\frac{1}{2}-[f(1-f)]^{1/2}}$ at $\Omega_c=\sqrt{\frac{1}{2}+[f(1-f)]^{1/2}}$. The upper + polarized mode takes its minimum value $(\Omega_{\rm up}^{(+)})_{\rm min}=\sqrt{\frac{1}{2}+[f(1-f)]^{1/2}}$ at $\Omega_c=\sqrt{\frac{1}{2}-[f(1-f)]^{1/2}}$. In a scarce square lattice of antidots the gap between the upper and lower + branches equals

$$(\Omega_{\rm up}^{(+)})_{\rm min}-(\Omega_{\rm low}^{(+)})_{\rm max}\approx(2f)^{1/2}=(2\pi)^{1/2}R/a\ ,\quad f\ll 1\ . \tag{29}$$

We suppose that, due to the small oscillator strength, the mode $\omega_{\rm up}^{(-)}$ was not observed in experiments.[9,10] Experimentally observed modes are the + polarized collective modes $\omega_{\rm up}^{(+)}(B)$ and $\omega_{\rm low}^{(+)}(B)$. As a whole, EMA results are in a good qualitative agreement with experiment. Two main features of the antidot spectrum noted in Refs. 9 and 10—the exchange of oscillator strength of the two main excitation branches and negative B dispersion of the high-frequency mode at small B—are seen in Fig. 4. In Fig. 3(b), two main + polarized excitation branches $\omega_{\rm up}^{(+)}(B)$ and $\omega_{\rm low}^{(+)}(B)$ are shown with experimental points of Ref. 9, sample (b). The value of ω_0 has again been found by fitting the $\omega_{\rm low}^{(+)}(B)$ curve to experimental data. The obtained value for $\omega_0^{\rm EMA}=2.17\times10^{13}\ {\rm s}^{-1}$ is in a reasonable agreement with both MDA results and calculated values (see above).

The EMA has the advantage that it gives a correct *qualitative* picture of the excitation spectrum of an inhomogeneous 2D antidot medium. However, it is not quite adequate for a *quantitative* description of all excitation branches. As seen from Fig. 3(b), an agreement between the high-frequency branch $\omega_{\rm up}^{(+)}(B)$ and experimental points is not so good [experimental data of Ref. 12 for mode $\omega_{\rm up}^{(+)}(B)$ were found to agree well with EMA results]. We suppose that the reason for this is in a rough, frequency-independent account of interantidot interaction in the EMA. One can show that the EMA would be valid if an induced potential would be proportional to $1/r$ at $r\gg R$ at all frequencies. As seen from the actual asymptotes of $\varphi_{\pm}^{\rm ind}(r)$, Eqs. (9) and (11), the EMA overestimates the interaction when it is small (at $\omega<\omega_c$) and underestimates it when it is large (at $\omega>\omega_c$). Indeed, at $\omega<\omega_c$ and $\omega_c\gg\omega_0$ (the interaction is small), the EMA give a larger correction to the EMP frequency ($\propto f$) [Eq. (28)] than the MDA ($\propto f^{3/2}$). When the frequency tends to the cyclotron one and interantidot interaction increases, the EMA and MDA give similar results [compare Eqs. (28) and (22) at $f\ll1$]. At $\omega>\omega_c$ the EMA plays the role of a tight-binding approximation for strongly interacting antidots. In the opposite limit of weak binding, the square lattice of antidots can be considered at $f\ll1$ as a point grid imposed on the homogeneous 2D electron layer. Due to the grid, 2D bulk magnetoplasmons with the frequency $\omega_{mp}(q=2\pi/a)$ are excited in the system. The branch $\omega=\omega_{\rm mp}(2\pi/a)$ is shown by the dashed-dotted curve in Fig. 3(b). Experimental points lie in between the theoretical curves corresponding to the EMA and the weak-binding approximation. This indicates that the EMA underestimates an interaction at $\omega>\omega_c$, and that an intermediate-binding case was actually realized in experiment. It should also be noted that, strictly speaking, the spatial ordering of antidots in square lattice is not taken into account in the EMA (resonance frequencies depend only on the space-average filling factor f of the system). In this respect the EMA is similar to the variational Wigner-Seitz approach.[14] It is probably a suitable model for a system with a random distribution of antidots over 2D space. An acceptor-doped 2D electron system with randomly distributed negatively charged centers[23] is an example of such a structure.

The presence of a CR line in the FIR spectrum is a peculiar feature of antidot systems. In the spectrum of dots the CR line is not observed due to the depolarization effect.[1] In antidots, depolarization fields are essential only inside and in some vicinity of antidots. At a large distance from them, electrons do not feel depolarization fields. This is qualitatively supported by comparison of data of Refs. 9 and 10. In Ref. 10, where the macroscopic electric fields were screened by metal gate, an oscillator strength of the CR line was relatively larger than in Ref. 9, where an etched structure without screening electrodes was used. Two contributions to excitation spectrum, demonstrated by the MDA expression (21), are conditioned by electrons which feel (collective contribution)

and do not feel (single-particle CR) depolarization fields. Contrary to the MDA, the single-particle CR line is not seen in the EMA absorption spectrum, Fig. 4(a). We believe that this is also a consequence of a rough inclusion of interantidot interaction in the EMA. The frequency-independent EMA asymptote $\varphi_{\pm}^{\rm ind}(r) \propto 1/r$ plays the role of a relatively strong depolarization field acting on electrons between antidots. As a result, the single-particle CR line is suppressed in the EMA.

In our theory we have neglected spatial dispersion effects. If the mean free path is large compared with the antidot lattice period a, the nonlocal effects can influence calculated spectra if $qv_F > |\omega - n\omega_c|$, where $n = 1,2,\ldots$, v_F is the Fermi velocity and $q^{-1} \approx a$ is the characteristic length of the electric-field variation in the system. An observed anticrossing of the upper excitation branch with a $2\omega_c$ harmonic of the CR was explained in Ref. 9 by nonlocal effects. A similar anticrossing due to nonlocal effects could be expected at $\omega \approx \omega_c$. Under the conditions of experiments in Refs. 9 and 10 the role of interantidot interaction is more important: the value of the expected nonlocal gap $\Delta\omega_{\rm nl} \cong v_F/a$ is much smaller than the gap $\Delta\omega_{\rm int} \cong \omega_0 R/a$ [Eq. (29)], conditioned by interantidot interaction, $\Delta\omega_{\rm nl}/\Delta\omega_{\rm int} \cong \sqrt{a_B^*/R} \ll 1$, where a_B^* is the effective Bohr radius.

The third region where nonlocal effects could modify our results is in the limit of small B and low frequency, $\omega_c < v_F/a$, $\omega < v_F/a$. Effects of commensurate electron orbits spanning one or several antidots observed in transport experiments[24,25] may manifest themselves in collective excitation spectra in this region. To confirm this, the spatial dispersion of conductivity should be taken into account.

V. SUMMARY

We have presented a theory of collective excitations in a single antidot and in a system of interacting antidots. In the single antidot, we have found two collective modes $\omega_{\rm CR}(B)$ and $\omega_{\rm EMP}(B)$. The first collective mode coincides with the single-particle CR line. The second mode has a sense of the edge magnetoplasmons localized near the boundary of antidots. An important feature of the single antidot spectrum consists of the absence of weakly damped collective modes at $\omega > \omega_c$. This is conditioned by the strong nondissipative damping of single antidot excitation modes due to the emission of 2D bulk magnetoplasmons. A similar effect should be the case in a dotlike structure,[26] where a disk with electron density n_i is immersed in the 2D layer with the smaller electron density $n_e < n_i$.

An important consequence of emission of 2D bulk magnetoplasmons by the antidot dipole at $\omega > \omega_c$ is that the interantidot interaction is of crucial importance in systems of antidots. Contrary to a system of dots, interantidot interaction *must be taken into account* even in a scarce lattice of antidots. To take the interantidot interaction into account we have used two approximations, the MDA and EMA. The EMA gives a good qualitative description of experimentally observed FIR absorption and excitation spectra. Both approximations agree quantitatively with experimental data for the low-frequency antidot mode.

ACKNOWLEDGMENTS

One of the authors (S.M.) acknowledges the International Science Foundation for support of this work (Grant Nos. RL6000 and RL6300). The other author (V.V.) thanks the financial support of the Russian National Program "Surface atomic structures," Project No. 95-3.2.

APPENDIX

Analytic properties of the kernel $L(r,r';l)$ [Eq. (5)], depend on the position of the integrand pole $q = q_0(\omega) = -1/l(\omega)$ in the complex q plane. At $\omega < \omega_c$ ($\omega > \omega_c$) the length $l(\omega)$ is positive (negative) and the pole $q_0(\omega)$ lies to the left (right) of the imaginary axis. Rewriting Eq. (5) in the form

$$L(r,r';l) = \int_0^\infty \frac{dq}{q+1/l} J_1(qr_<) H_1^{(1)}(qr_>) + \int_0^\infty \frac{dq}{q+1/l} J_1(qr_<) H_1^{(2)}(qr_>) ,$$

and rotating the integration path by the angle $\pi/2$ ($-\pi/2$) in the first (second) integral, we obtain

$$L(r,r';l) = 2\pi i \Theta[-{\rm Re}(l)] J_1(-r_</l) H_1^{(1)}(-r_>/l) + \frac{4r_>}{\pi l} \int_0^\infty \frac{dt}{t^2 + (r_>/l)^2} \cdot I_1(tr_</r_>) K_1(t) . \quad \text{(A1)}$$

Here I_1, K_1, $H_1^{(1)}$, and $H_1^{(2)}$ are the modified Bessel and Hankel functions, $r_< = \min\{r,r'\}$, and $r_> = \max\{r,r'\}$. If $\omega < \omega_c$, the first line in (A1) vanishes, and the asymptote of kernel $L(r,r';l)$,

$$L(r,r';l) = (2r_</\pi l) F(r_>/l), \quad r_</r_> \ll 1 , \quad \text{(A2)}$$

is determined by the function

$$F(z) = \int_0^\infty \frac{tdt}{t^2+z^2} K_1(t) \approx \begin{cases} \pi/2z & \text{at } 0 < z < 1 \\ \pi/2z^2 & \text{at } z \gg 1 , \end{cases} \quad \text{(A3)}$$

which can be interpolated at all $z > 0$ by the simple formula

$$F(z) \approx \frac{\pi}{2z(1+z)} . \quad \text{(A4)}$$

If $\omega \to \omega_c$ and hence $l(\omega) \to \infty$, $L(r,r';l \to \infty) = r_</r_>$. At $\omega > \omega_c$ the main contribution to the asymptote of $L(r,r';l)$ is made by the first line of Eq. (A1).

At $r = r'$ the function $L(r,r;l) \equiv S(r/l)$ is reduced to the tabulated integral[27]

$$S(z)=2\int_0^\infty \frac{dt}{t+z}J_1^2(t)=-\pi J_1(z)Y_1(z)-\frac{8z}{3\pi}\,{}_2F_3(1,1;\tfrac{3}{2},\tfrac{5}{2},\tfrac{1}{2};-z^2)$$
$$\equiv\left[1+\frac{8z}{3\pi[1+\gamma(z)]}\right]^{-1}. \tag{A5}$$

The function $\gamma(z)$ equals zero at $z=0$ and increases logarithmically at $z\to\infty$:

$$\gamma(z)\approx\begin{cases}(3\pi z/16)\{\ln(2/z)+[\psi(1)+\psi(2)]/2-\frac{1}{4}-2(8/3\pi)^2\}, & |z|\ll 1\\ (16/3\pi^2)[\ln(2z)-\psi(\frac{3}{2})]-1, & z\gg 1\ .\end{cases} \tag{A6}$$

Here J_1, Y_1, and ${}_2F_3$ are the Bessel, Neimann, and hypergeometric functions; and $\psi(3/2)=0.037$, $\psi(1)=-C$, and $\psi(2)=-C+1$, where $C=0.5772$ is the Euler constant.

*Present address: Institut für Theoretische Physik, Universität Regensburg, D-93040 Regensburg, Federal Republic of Germany. Electronic address: sergey.mikhailov@physik.uni-regensburg.de

[1]S. J. Allen, Jr., H. L. Störmer, and J. C. M. Hwang, Phys. Rev. B **28**, 4875 (1983).
[2]R. P. Leavitt and J. W. Little, Phys. Rev. B **34**, 2450 (1986).
[3]S. K. Yip, Phys. Rev. B **43**, 1707 (1991).
[4]A. O. Govorov and A. V. Chaplik, Zh. Eksp. Teor. Fiz. **99**, 1853 (1991) [Sov. Phys. JETP **72**, 1037 (1991)].
[5]V. Shikin, S. Nazin, D. Heitmann, and T. Demel, Phys. Rev. B **43**, 11 903 (1991).
[6]L. Brey, N. F. Johnson, and B. I. Halperin, Phys. Rev. B **40**, 10 647 (1989).
[7]V. A. Volkov and S. A. Mikhailov, Zh. Eksp. Teor. Fiz. **94**, 217 (1988) [Sov. Phys. JETP **67**, 1639 (1988)].
[8]D. Heitmann, K. Kern, T. Demel, P. Grambow, K. Ploog, and Y. H. Zhang, Surf. Sci. **267**, 245 (1992).
[9]K. Kern, D. Heitmann, P. Grambow, Y. H. Zhang, and K. Ploog, Phys. Rev. Lett. **66**, 1618 (1991).
[10]Y. Zhao, D. C. Tsui, M. Santos, M. Shayegan, R. A. Ghanbari, D. A. Antoniadis, and H. I. Smith, Appl. Phys. Lett. **60**, 1510 (1992).
[11]A. Lorke, J. P. Kotthaus, and K. Ploog, Superlatt. Microstruct. **9**, 103 (1991).
[12]A. Huber, I. Jejina, H. Lorenz, J. P. Kotthaus, S. Bakker, and T. M. Klapwijk, Semicond. Sci. Technol. **10**, 365 (1995).
[13]V. Fessatidis, H. L. Cui, and O. Kühn, Phys. Rev. B **47**, 6598 (1993).
[14]G. Y. Wu and Y. Zhao, Phys. Rev. Lett. **71**, 2114 (1993).
[15]A. Lorke, Surf. Sci. **263**, 307 (1992).
[16]K. Tevosyan and V. Shikin, Zh. Eksp. Teor. Fiz. **104**, 4121 (1993) [Sov. Phys. JETP **77**, 993 (1993)].
[17]C. Dahl, J. P. Kotthaus, H. Nickel, and W. Schlapp, Phys. Rev. B **46**, 15 590 (1992).
[18]We do not consider the radiation of transverse electromagnetic waves by antidot dipole in this paper.
[19]V. A. Volkov and S. A. Mikhailov, in *Modern Problems in Condensed Matter Sciences,* edited by V. M. Agranovich and A. A. Maradudin (North-Holland, Amsterdam, 1991), Vol. 27.2, Chap. 15, p. 855.
[20]In numerical estimations we use the parameters of the sample (b) from Ref. 9: $n_s=2.5\times10^{12}$ cm^{-2}, $\kappa=13.7$, $a=300$ nm, $R=50$ nm, and $h\leq 30$ nm, so that $h/R\leq 0.6$ and $f=0.087$.
[21]Nonlocal effects will also give rise to an anticrossing of modes. Under the conditions of experiments (Refs. 9 and 10), the role of interantidot interaction is more important.
[22]S. A. Mikhailov and V. A. Volkov, Phys. Low-Dim. Struct. **1**, 31 (1994).
[23]J. Richter, H. Sigg, K. von Klitzing, and K. Ploog, Surf. Sci. **228**, 159 (1990).
[24]K. Ensslin and P. M. Petroff, Phys. Rev. B **41**, 12 307 (1990).
[25]D. Weiss, M. L. Roukes, A. Menschig, P. Grambow, K. von Klitzing, and G. Weimann, Phys. Rev. Lett. **66**, 2790 (1991).
[26]S. A. Mikhailov and V. A. Volkov, J. Phys. Condens. Matter **4**, 6523 (1992).
[27]A. P. Prudnikov, Yu. A. Brychkov, and O. I. Marichev, *Integrals and Series: Special Functions* (Nauka, Moscow, 1983), Vol. 2, p. 212 (in Russian).

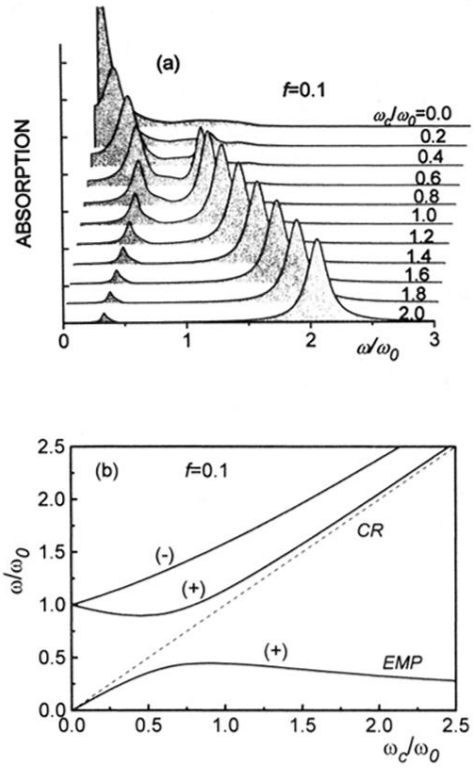

FIG. 4. FIR absorption (a) and excitation (b) spectra of a system of antidots in the EMA at $f=0.1$. (+) and (−) signs in (b) label the polarization of modes.